Composite Structures 208 (2019) 377–384

Contents lists available at ScienceDirect

Composite Structures

journal homepage: www.elsevier.com/locate/compstruct

Dynamic response of flexible hybrid electronic material systems

Nicholas C. Sears[a], John Daniel Berrigan[b], Philip R. Buskohl[b], Ryan L. Harne[a,*]

[a] Department of Mechanical and Aerospace Engineering, The Ohio State University, Columbus, OH 43210, USA
[b] Soft Materials Branch, Materials and Manufacturing Directorate, Air Force Research Laboratory, Wright Patterson Air Force Base, OH 45433, USA

ABSTRACT

Flexible hybrid electronic (FHE) material systems embody the intersection of compliant electrical networks and functional material architectures. For a wide variety of future applications, FHE material systems will be subjected to dynamic mechanical stresses, such as for motion monitoring or for vibration isolation. Consequently, an understanding is required on how these new classes of material systems may respond mechanically and electrically when under states of high-cycle and high-frequency loads. Here, conductive silver microflake ink is interfaced with elastomeric geometries programmed with specific strain responses. Changes in electrical resistance under cyclic displacements are shown to depend on the heat generated by electrical current flow and on the thermal heat generation promoted by the pre-strain on the material system. Configurations subject to high static pre-strains and large strain rates exhibit greater increases in temperature and resistance, whereas a near constant conductivity is manifest in FHE material systems with compositions that reduce static local strains despite high engineering pre-strain application. These results may guide future efforts to understand the resistance change in conductive ink networks and expand the use of flexible hybrid electronic material systems into myriad dynamic application environments.

1. Introduction

Research into flexible hybrid electronics (FHEs) has flourished due to the new opportunities made possible by the introduction of compliance into electronic components. FHEs have been implemented in fields ranging from human health monitoring to soft robotics for the ability to conduct electrical signals while undergoing large strain [1]. FHEs can be composed of a network of conductive flakes or particles embedded in a flexible material matrix [2–4], which together constitute conductive inks that serve as compliant, electrical conduits [4–6]. Conductive ink-based FHEs have been formulated with a variety of metal flakes or particles, including copper [5], gold [6], and silver [4]. Typical polymers for the material matrix of the inks include thermoplastics due to desirable flexibility [4]. The dispersion of conductive flakes or particles within a polymer matrix creates a flexible and conductive percolating network in which overall conductivity is determined by the proximity of contact between the microscale conductive constituents [7].

Despite the flexibility that FHEs provide, a disruption of the conductive network through mechanical or thermal stresses may result in a reduction of electrical conductivity and thus reduction of operational effectiveness. In light of this, there has been an interest to characterize and understand the mechanisms that contribute to changes of the conductivity of such networks. For example, large strains [8,9] and high strain rates [10,11] can disrupt the conductive network through stress that may physically separate previously adjacent conducting particles. Similarly, temperature changes within electrically conductive networks can result in thermal stresses due to the different thermal expansion properties of the conductive constituents and the polymer matrix [12]. Large temperature fluctuations during fabrication [13] or the heat generated by electric currents [12] have also demonstrated a disruption of current flow via the thermal stress. Thermal imaging has revealed direct evidence of how the current flow through electrically conductive networks is influenced by the state of microstructural stress and strain [14].

In certain cases, the sensitivities of FHEs to stress and strain are exploited for functional applications that are unachievable with conventional electronics. For example, conductive inks may be leveraged to detect or measure strain through resistance changes that occur as a result of a change in the strained conductive network [4,15–17]. Interest in FHE 'wearables' has stimulated attention to methods of harnessing FHEs to monitor muscle movements in speech [18] and heart rate [19]. Still, the full scope of opportunities for FHEs to build upon the capabilities of conventional electronics has yet to be explored.

For instance, the influence of dynamics, such as high frequency cyclic forces, on the conductivity of conventional wired electronics is well known [20,21]. This has inspired the use of tunable elastomeric material systems that leverage large deformation of microscopic structural geometries to mitigate vibration energy transfer [22,23]. With the elastomer matrix of conductive ink based FHEs, similar opportunities may exist for FHEs to enhance the capabilities of conventional electronics by combining protective and electrically conductive

* Corresponding author.
E-mail address: harne.3@osu.edu (R.L. Harne).

https://doi.org/10.1016/j.compstruct.2018.10.023
Received 30 May 2018; Received in revised form 3 October 2018; Accepted 8 October 2018
Available online 09 October 2018
0263-8223/

functions. Therefore, the use of conductive ink-based FHEs within geometries designed for vibration and shock energy mitigation presents an ideal opportunity to create FHE material systems and investigate behaviors manifest in dynamic excitation environments.

In order to achieve an understanding of how FHE material systems may respond under dynamic loads, there is a need to account for and monitor transient behavior that may influence mechanical and electrical properties. Furthermore, it is important to uncover how transient behavior may change with varying static strain distributions manifest in compressed FHE material systems [14]. For example, thermoplastics are a common material of choice for the elastomer material matrix of FHEs [24]. Yet the inherent viscoelasticity results in strain transfer characteristics that depend upon the static and dynamic states of mechanical stress [25]. Thermoplastics also exhibit softening under low frequency cyclic displacements due to the Mullin's effect [24] and the softening may be attributed to internal temperature rise from high frequency mechanical loads [25–27]. Additionally, filler particles within thermoplastics contribute to the accumulation of internal heat [27], which may be significant when considering the effects of embedded metal flakes under strain in thermoplastics. Therefore, the cumulative influence of these behaviors on the electrical conductivity of FHE networks in material systems subjected to high frequency dynamic loads is important to uncover.

Summarizing the state-of-the-art understanding of FHE properties adaptation resulting from mechanical loads, changes in static strain and stress distinctly tailor the microstructural characteristics of FHE networks, which influence electrical conductivity. Yet, the nuanced mechanisms that contribute to the precise electrical response under dynamic mechanical loads are unknown. Therefore, this research seeks to reveal how the static strain characteristics of conductive networks embedded in material systems contribute to electrical conductivity and mechanical behaviors under dynamic stresses. Because a wide variety of applications that may deploy FHEs involve relatively low frequency harmonic stresses, such as at frequencies 50 Hz and less, this research gives priority attention to this frequency regime.

This report is organized as follows. In Section 2, the FHE material systems fabricated and modeled here are described in detail. Then, in Section 3, a comprehensive investigation into the underlying physics of electrical resistance change within conductive inks undergoing dynamic excitation is given. Finally, in Section 4, a summary of the findings of this research and implications are presented.

2. Specimen descriptions and investigative methods

2.1. Specimen descriptions

In order to investigate the dynamic behaviors of FHE material systems potentially suitable for vibration mitigation practices, two material system compositions are studied. Fig. 1(a) and (b) respectively show the ‘strain-sensitive’ and ‘strain-insensitive’ material systems. In this work, the mechanical and electrical behaviors of the material systems are caused by uniaxial applied displacement from the vertical direction according to the orientation of Fig. 1. Considering the loading axis, the strain-sensitive specimen of Fig. 1(a) is used to investigate the dynamic influences on conductive ink traces interfaced with geometries that maximize strain transfer to the ink trace by the snap-through response of the vertically-oriented buckling beam-like member [28]. In contrast, the strain-insensitive specimen in Fig. 1(b) is used to investigate the dynamic influences on conductive ink traces interfaced with geometries that may limit significant strain transfer to the conductive ink trace through more gradual collapse of the geometry caused by the applied displacement [29].

The FHE material systems shown in Fig. 1(a) and (b) represent diverse compositions that permit close study of electrical characteristics of conductive inks subjected to static pre-strain and dynamic mechanical loads. For this research, an ink composed of silver (Ag) microflakes embedded in a thermoplastic polyurethane (TPU) matrix is prepared (Ag-TPU ink). The electrical resistance of the Ag-TPU ink is measured through wire leads, as shown in Fig. 1(a) and (b). The specimen geometries are composed of a commercial 3D printed, thermoplastic polymer (Stratasys material Tangoblackplus, FLX980). For more information regarding the preparation and fabrication of the specimens, see Supporting Information Section 1.

2.2. Experimental methods and FE model description

The dynamic properties of the FHE material systems shown in Fig. 1 are evaluated at engineering pre-strains ε, defined as the applied displacement over initial specimen height. The three values of pre-strain used to examine the FHE material systems of this work are selected to characterize the buckling behavior of the strain-sensitive specimen: pre-buckled, near the buckling point, and post-buckled. These configurations correspond to engineering pre-strains of ε = 4%, 8%, and 14%, respectively. These pre-strain magnitudes are used to investigate the strain-sensitive and strain-insensitive specimens, respectively shown in Fig. 2(a) and (b).

At each of the static pre-strain configurations shown in Fig. 2(a) and (b), the specimens are subjected to sinusoidal displacements applied by an electrodynamic shaker (LDS V408) that is controlled by a controller (Vibration Research VR9500) and amplifier (Crown XLS1500). As the specimen undergoes harmonic displacement input, the input and output dynamic forces are measured by a matched pair of force transducers (PCB 208C01) that start and terminate the loading fixture. The conductive ink trace resistance is simultaneously monitored with a voltage divider circuit. The components of the experimental setup are labeled in Fig. 2(a). This experimental setup is employed to characterize how the mechanical and electrical properties are influenced by the pre-strain and applied dynamic displacements at frequencies of 50 Hz and less.

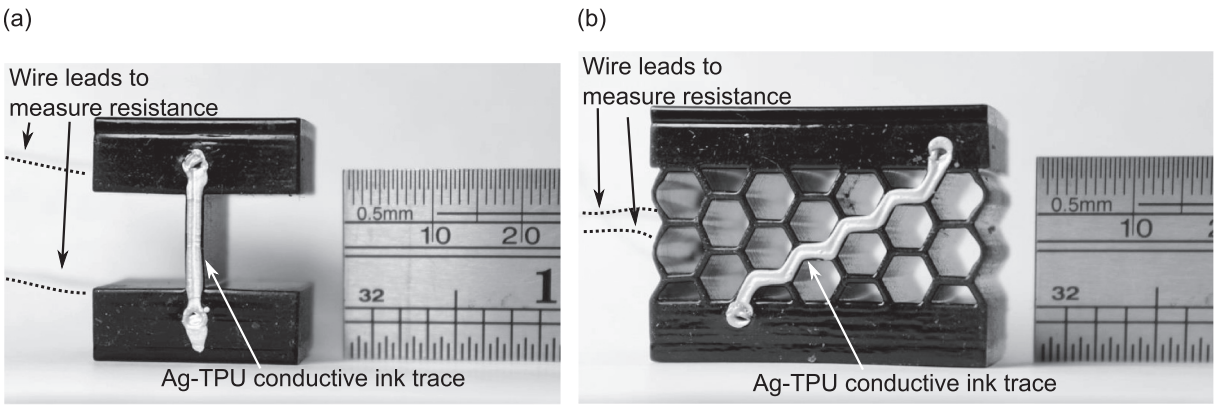

Fig. 1. (a) Strain-sensitive and (b) strain-insensitive specimens with conductive ink traces and wire leads to measure resistance.

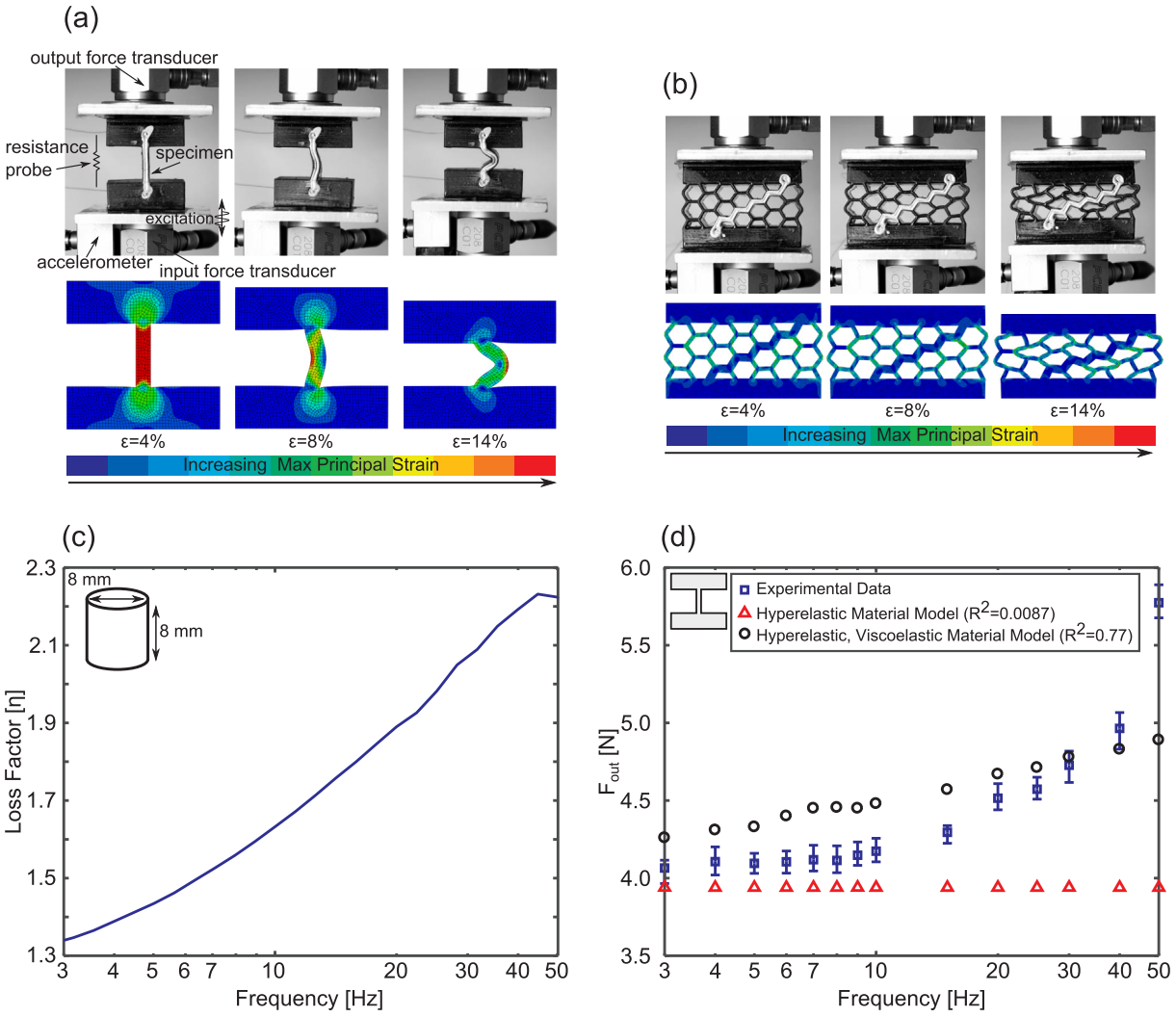

Fig. 2. (a) Strain-sensitive specimen, with experimental setup indicated, and (b) strain-insensitive specimen with FE model static pre-strain deformation shapes, colored according to maximum principal strain at engineering pre-strains ε = 4%, 8%, and 14%. (c) Comparison of average output force for 0.25 mm peak-to-peak excitation applied at frequencies between 3 and 50 Hz for experiments, a hyperelastic model, and a hyperelastic and viscoelastic model. Maximum and minimum measurements are indicated by range bars.

This represents a frequency range indicative of potential applications of FHE materials systems as wearables, self-sensing elastomers and mounts, motion sensors, among other applied contexts. Resonance in the strain-sensitive and strain-insensitive specimens occurs at frequencies in the 1000 s of Hz, where viscoelastic damping dominates and suppresses unique dynamic behaviors. Consequently, the low frequency, sub-resonant regime with dynamic stresses of 50 Hz and less is considered in this investigation as the loading environment for the material systems.

In order to model the mechanical behaviors of the specimens observed in experiments, two-dimensional (2D) plane strain, finite element (FE) models of the specimens are generated in ABAQUS. A Neo-Hookean, hyperelastic material model serves as the basis for the FE model by providing the necessary material properties of the specimens. The hyperelastic material model uses the following properties that are empirically identified: density $\rho = 1112\,\mathrm{kg.m^{-3}}$, Poisson's ratio $\upsilon = 0.49$, shear modulus $\mu = 248$ kPa, and bulk modulus $\kappa = 16.6$ MPa. Additionally, in order to model the frequency and time dependent influences observed experimentally, a Prony series, viscoelastic material model is utilized. Details about the Prony series coefficient identification procedure is given in the Supporting Information Section 2. For the FE modeling of the dynamic loading experiments, a two step procedure is employed. First, a dynamic-implicit model formulation applies static pre-strain to specimens, while a second dynamic-explicit study step applies the harmonic displacement input. In order to replicate experiments, one side of each specimen is fixed (output side) while pre-strains and harmonic displacements are applied to the opposite end (input side). Self-contact by tangential friction penalty coefficient of 90% is applied to all edges of the 2D FE model domain. Prior to obtaining final results for processing, a mesh convergence study with CPS4R elements is undertaken to ensure that the FE model outcomes are consistent in quantitative values by a suitably refined mesh.

As shown in Fig. 2(a) and (b), the static deformation of the specimen configurations in experiments is accurately reconstructed by the FE model. In the FE model results of Fig. 2(a,b), the shading is colored according to maximum principal strain. The agreement between the static deformations observed experimentally and computationally for the strain-sensitive and -insensitive specimens in Fig. 2(a) and (b), respectively, indicates that the static strain distributions identified by the FE models may likewise be accurate representations.

In Fig. 2(c), for a 0.25 mm peak-to-peak applied harmonic displacement, average experimental data is shown according to data markers with range bars indicating maximum and minimum measurements across three separate experiments. Experimental results show an increase in output force with frequency of the applied displacement. Furthermore, as shown in Fig. 2(c), for a 0.25 mm peak-to-peak applied

harmonic displacement, the hyperelastic and viscoelastic material model shows increasing average output force under dynamic excitation, compared to a hyperelastic model that is frequency independent. The combined hyperelastic and viscoelastic material model exhibits a stronger correlation to experimental data (R^2 = 0.77) than the hyperelastic material model alone (R^2 = 0.0087). Thus, the addition of the viscoelastic material model is essential to the exploration of the stress, strain, and deformation dynamics of these specimens and matches well with experiments. The combined hyperelastic and viscoelastic material model is used in the ensuing FE investigations that augment and elucidate experimental findings.

3. Results and discussion

3.1. High-cycle and high-frequency loading influences on FHE material system behaviors

In order to evaluate the FHE material systems under high frequency dynamic mechanical loads, specimens undergo cyclic displacement experiments. For these experiments, a 0.25 mm peak-to-peak displacement is applied at a 25 Hz excitation frequency to specimens under the pre-strains identified in Fig. 1(a) and (b) for 10,000 displacement cycles. Before dynamic excitation is applied, specimens are allowed to come to electrical equilibrium until the pre-strained specimen resistance measurements are approximately constant, which typically occurs within 10 min under static stress conditions. At this time, initial electrical resistance measurements corresponding to each configuration are recorded and reported as R_0.

As shown in Fig. 3(a) and (b), the force transfer function computed as the ratio of dynamic output force to dynamic input force, increases by less than 0.8% for all specimens and configurations by displacement cycle 10,000. On the other hand, the trends in resistance change in Fig. 3(c) and (d) differ among the specimen geometries and pre-strain configurations. As shown in Fig. 3(c), the resistances of the conductive ink trace in ε = 4% and 8% configurations of the strain-sensitive specimen show a 35% and 8% increase in resistance by displacement cycle 100, respectively, followed by gradual increases in resistance over the duration of the experiments. Yet, the resistance of the conductive ink trace in the ε = 14% configuration does not indicate sudden resistance increase after 100 displacement cycles, and in fact gradually decreases in resistance value over the remaining duration of the experiment. For the strain-insensitive specimen, the resistances of the conductive ink traces remain nearly constant over the duration of the experiment for all configurations, as shown in Fig. 3(d).

Previous studies have revealed that conductive networks may be disrupted by the application of an instantaneous stress, which results in an increase in initial resistance [30,31]. The application of an instantaneous stress is generated at the beginning of each experiment with the onset of harmonic displacement. Such stress may explain the large increases in resistance associated with the strain-sensitive specimen for pre-strain conditions ε = 4% and ε = 8%. This is explored for the specimens in this research in greater detail with the use of FE simulations in Supporting Information Section 2 to help elucidate the behaviors observed in Fig. 3(c,d). It is found that greater peak stress

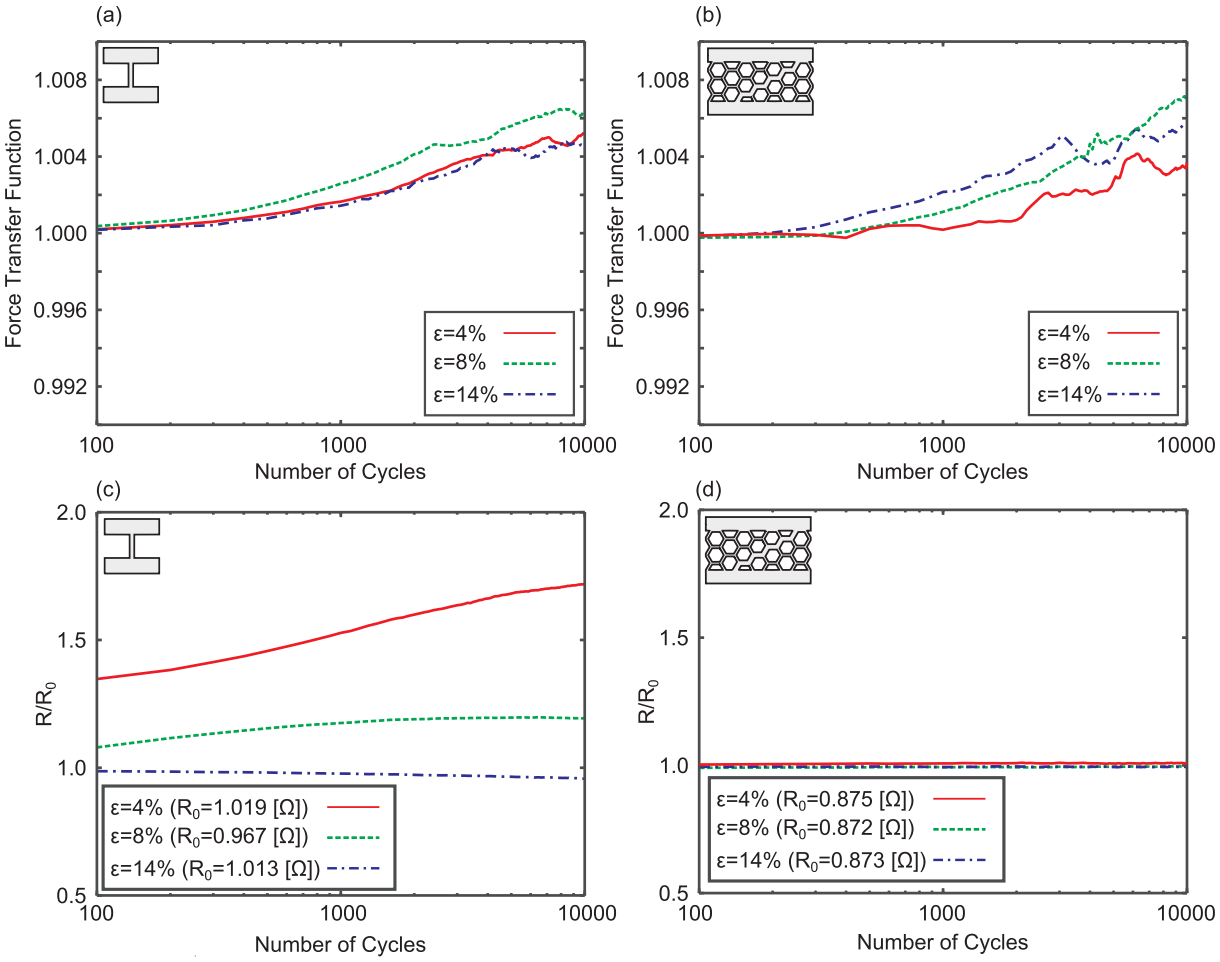

Fig. 3. Force transfer function is shown for ε = 4%, 8%, and 14% configurations of the (a) strain-sensitive and (b) strain-insensitive specimens for a 10,000 cycle displacement experiment with 0.25 mm peak-to-peak applied displacement. Normalized resistance change is shown for ε = 4%, 8%, and 14% configurations of the (c) strain-sensitive and (d) strain-insensitive specimens.

changes within the conductive ink traces are associated with greater initial resistance changes, which may explain the trends in Fig. 3(c,d) for the respective relative resistance change for the FHE material systems. On the other hand, a greater number of influences may still collectively yield such behaviors seen in Fig. 3(c,d), so that future work is desired.

Resistance changes in conductive networks under cyclic mechanical loading have previously been characterized with respect to low frequency excitations, wherein the findings reveal increases in electrical resistance due to accumulated disruptions of the conductive network [8,32]. Therefore, a need remains to explain the resistance trends of Fig. 3(c,d) that are shown to increase, decrease, or remain constant as the number of high frequency displacement cycles increases. To this end, an investigation is needed to study the influences of static pre-strain on the electrical resistance during cyclic displacement experiments.

3.2. Heat generation influence on resistance change

Mechanical strains can cause electrical resistance changes in FHEs through disruptions of the conductive network [4,15–17]. For instance, supporting experiments undertaken here exemplify the visible destruction to the conductive ink network before and after the application of a static pre-strain, as shown in Supporting Information Section 3. Yet, research into the failure mechanisms of silver microflake-based electrical connections under thermal and mechanical influences shows that the efficacy of the conductive network is also strongly influenced by temperature [33]. Although temperature is not usually considered in cyclic deformation experiments of FHEs, the use of thermoplastics in the FHE material systems studied here may cultivate relevant thermoelastic phenomena under high frequency mechanical loads [27], while heat generated due to electric currents passing through the conductive ink traces cannot be neglected [12]. In order to explore the influence of temperature changes within the conductive ink traces, average ink trace temperatures are measured with a thermal imaging camera (FLIR C2) during cyclic displacement experiments. Before each experiment, specimens are allowed to come to thermal and electrical equilibrium. At this time, average ink trace temperatures and resistances are measured to record baseline, constant values. Thermal images are shaded with coloring according to temperature changes from -2 to $+7$ degrees C, with respect to the baseline temperature distributions.

Thermal images of the specimens are shown for displacement cycles 0 and 10,000 for each pre-strain configuration, Fig. 4(a,c). As shown in Fig. 4(a) for the strain-sensitive specimen, heat is noticeable within the conductive ink traces before and after experiments due to passing small, constant electrical current used for the resistance measurement in the voltage divider circuit. The largest temperature changes of the strain-sensitive specimen appear to be concentrated within the conductive ink traces as well. For instance, the conductive ink traces in $\varepsilon = 4\%$ and $\varepsilon = 8\%$ configurations of the strain-sensitive specimen show significant heat generation in Fig. 4(a), indicated by changes in color according to the temperature change scale. Furthermore, as is most clearly exemplified by the $\varepsilon = 4\%$ strain-sensitive specimen, the input side of the specimen that is dynamically displaced by the input, corresponding to the bottom of the specimen as shown in Fig. 4(a), experiences a larger increase in temperature than that of the output side. Larger increases in temperature for the input sides of the specimens compared to the output sides may explain the increases in transfer function seen in Fig. 3(a) and (b) due to a softening effect of elastomers that occurs with internal heat generation [25,26]. In other words, a softening of output force with a greater softening of input force results in an increase in output-to-input transfer function over the duration of the experiment. In fact, this hypothesis is supported by complementary data in the Supporting Information Section 4 wherein the FHE material systems without conductive traces are also dynamically displaced at 25 Hz for 10,000 displacement cycles and likewise show steady transfer function increase with increase in displacement cycles. Yet, as shown in Fig. 3(a) and (b), these changes are relatively minor and result in a less than 0.8% change in transfer function for both specimens.

Although the force transfer functions of the experimental specimens may change only slightly due to internal heat generation, the thermoelastic heat generation properties of the conductive ink may influence electrical resistance in a more significant way. For instance, polymers with added fillers such as silver have been shown to possess greater thermal conductivity than those of the unfilled polymer. In this way, the conductive ink traces may conduct more heat than the elastomer of the specimen geometry [34]. It has been shown that large temperatures can disrupt conductive networks through thermal fatigue cracking and accumulated strain [33]. This results in a degradation or failure of the conductive networks [12,13]. The thermoelastic heat generation in conductive ink traces is thought to be due to the thermal stresses associated with two materials of different thermal expansion coefficients [12]. Thus, it may be concluded that temperature changes within the conductive ink traces, composed of metal microflakes within a thermoplastic material matrix, result in the resistance changes measured during cyclic displacement experiments.

Indeed, as shown in Fig. 4(b), changes in average ink trace temperature of $+5.3$ and $+2.8$ degrees C are measured for the $\varepsilon = 4\%$ and $\varepsilon = 8\%$ configurations of the strain-sensitive specimen, respectively. On the other hand, a change in average ink trace temperature of -0.5 degrees C is measured for the $\varepsilon = 14\%$ strain-sensitive specimen. These thermal and electrical behaviors contrast greatly with the results obtained for the strain-insensitive specimen. Fig. 4(c) shows thermal images at displacement cycles 0 and 10,000 for the strain-insensitive specimen. Heat is concentrated within the conductive ink traces before and after experiments, mostly associated with the electric current flow. Yet, unlike the $\varepsilon = 4\%$ and 8% configurations of the strain-sensitive specimen, all configurations of the strain-insensitive specimen show little to no heat generation within the conductive ink trace by displacement cycle 10,000. Measurements of the average conductive ink trace temperature of the strain-insensitive specimen in Fig. 4(d) show temperature changes of $+0.5$, $+0.6$, and -0.9 degrees C for $\varepsilon = 4\%$, 8%, and 14% configurations, respectively.

The thermal images in Fig. 4(a,c) and average temperature changes of Fig. 4(b,d) suggest that the extent to which thermal stress is generated within the ink traces may be determined in part by specimen configuration that corresponds to the local, static strain in the conductive ink trace. For instance, as shown in the FE model deformation shapes of the strain-sensitive specimen in Fig. 2(a), the beam onto which the conductive ink trace is applied exhibits decreasing local principal strain with increasing compressive pre-strain for $\varepsilon = 4\%$, 8%, and 14% configurations. The state of local strain for $\varepsilon = 4\%$ and 8% configurations, under dynamic mechanical loads, generates heat through thermal stresses that disrupt the conductive network so as to contribute to the resistance changes at displacement cycle 10,000 of 72% and 20%, respectively, as shown in Fig. 3(c). On the other hand, the FE model deformation shapes of the strain-insensitive specimen in Fig. 1(b) show that all configurations of the strain-insensitive specimen exhibit smaller local, static principal strains in the conductive ink trace beam. Therefore, the strain-insensitive specimen experiences less thermal stress and exhibits average conductive ink trace temperature changes of less than 1 degree C in magnitude, as seen in Fig. 4(c,d). As a result, the strain-insensitive specimen shows negligible change in resistance over the duration of the experiment for all pre-strain configurations, Fig. 3(d).

Yet, temperature changes of less than 1 degree C, as measured for the strain-insensitive specimen in Fig. 4(d), are also measured for the $\varepsilon = 14\%$ strain-sensitive specimen, as shown in Fig. 4(b), and resistance decreases by 4% by displacement cycle 10,000, as shown in Fig. 3(c). This suggests that the resistance change of the $\varepsilon = 14\%$ strain-sensitive specimen may not be due to thermal stress. The decrease in resistance may be due to the increased conductivity associated with conductive

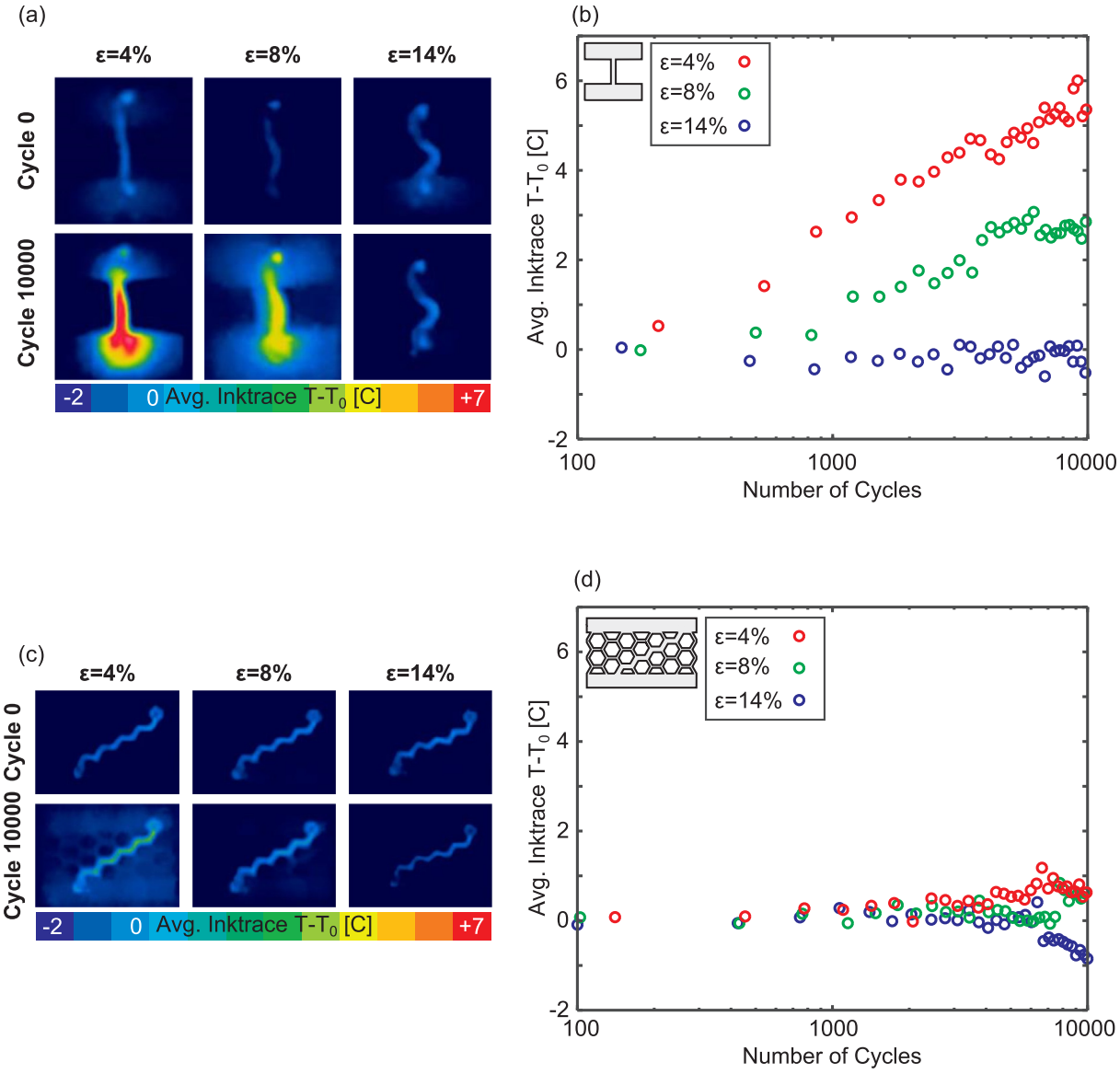

Fig. 4. Specimen architecture and deformation mode dictates intensity of thermal load. (a) and (c) Thermal images at displacement cycle number 0 and 10,000 for the strain-sensitive and strain-insensitive specimens, respectively. (b) and (d) Change in average temperature of conductive ink trace for all configurations of the strain-sensitive and strain-insensitive specimens, respectively.

networks under high strain. For instance, Busfield et al. [35] and Yamaguchi et al. [36] show that for conductive networks under quasi-static tensile strain, an increase in resistance, due to a disruption of the conductive network, can be followed by a decrease in resistance due to a rotational alignment of conductive particles induced by large strains. The highly deformed conductive ink trace beam in the $\varepsilon = 14\%$ configuration of the strain-sensitive specimen, as shown in Fig. 2(a), suggests that such unique realignment of conductive particles may be cultivated through highly deformed shapes and contribute to similar electrical behavior. Therefore, in the highly deformed configuration of the $\varepsilon = 14\%$ strain-sensitive specimen, the state of static pre-strain contributes to a decrease in electrical resistance with cyclic deformation, as shown in Fig. 3(c).

The many distinguishing resistance and temperature changes among specimens and geometric configurations highlights the intricate influences that static pre-strains have on the electrical behavior of the FHE material systems. Under dynamic mechanical loads, conductive ink traces in configurations of high static strain generate internal heat through thermal stresses. Thermal stresses, due to the viscoelasticity of the elastomer matrix and due to the thermal expansion mismatch between the elastomer matrix and embedded metal flakes, result in disruptions of the conductive network and increases in electrical resistance. On the other hand, conductive ink traces in configurations of low internal static pre-strain under dynamic mechanical excitation do not generate significant heat through thermal stresses and show negligible resistance change. It is also possible that conductive ink traces in highly deformed configurations, such as the strain-sensitive specimen subjected to $\varepsilon = 14\%$ pre-strain, may show decreasing electrical resistance with cyclic displacement, due to an induced re-alignment of the conductive network rather than thermal influences. Future research should investigate the movement of metal flakes within conductive ink traces in highly deformed configurations under dynamic excitation since these configurations may provide a unique combination of high static pre-strain and low thermal stress characteristics.

3.3. Frequency dependence on resistance change

In Section 3.2, the influence of dynamic mechanical excitation on

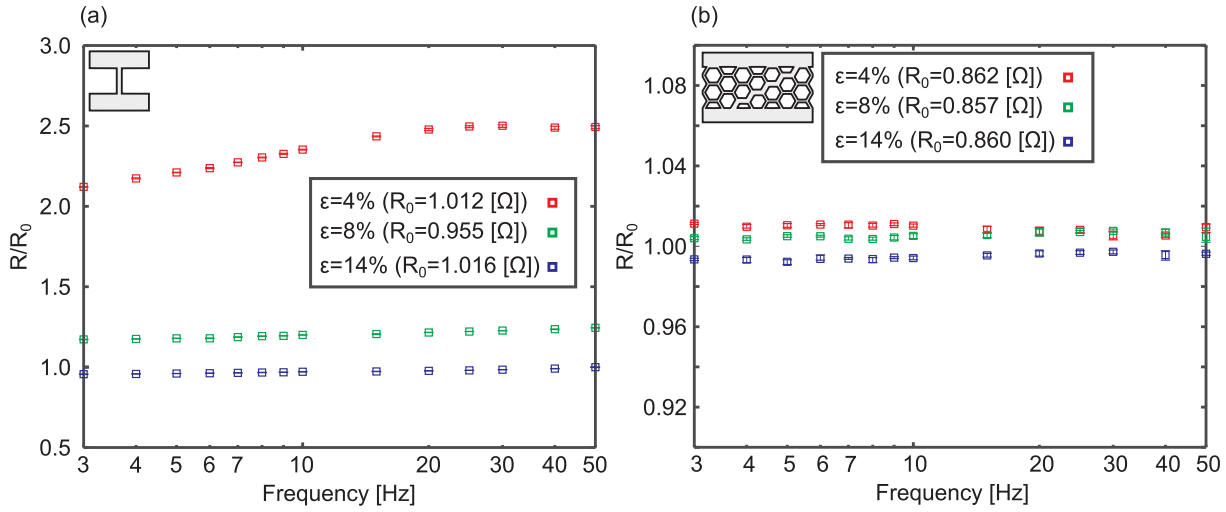

Fig. 5. Resistance change for specimen configurations evaluated at frequencies ranging from 3 to 50 Hz for (a) strain-sensitive and (b) strain-insensitive specimens.

the resistance changes of conductive ink traces in FHE material systems under pre-strains of ε = 4%, 8%, and 14% is investigated for a 25 Hz frequency of applied displacement cycles. In order to understand how FHEs respond under high frequency dynamic loads, it is important to consider the effects that the loading frequency may have on the electrical resistance behavior. This is evident when considering the influence of displacement excitation frequency on the average output force shown in Fig. 2(d). In order to investigate the influence of loading frequency on FHE material systems, the resistances of the specimen ink traces are measured over 20 s time intervals at frequencies ranging from 3 to 50 Hz and with a 0.25 mm peak-to-peak amplitude of applied displacement. Measurements are taken 2 min after excitation begins to allow the specimen to come to a pseudo-steady state of resistance change. Additionally, specimens are allowed to come to electrical equilibrium where resistance measurements are constant before each experiment. These equilibrated resistances are denoted as R_0. The data markers in Fig. 5 correspond to the average resistance measured during the 20 s time interval, while the range bars indicate the maximum and minimum resistance measurements taken during that time period.

As shown in Fig. 5(a) for the strain-sensitive specimen, changes in electrical resistance of +112%, +17%, and -4% are measured at a 3 Hz displacement excitation frequency for the ε = 4%, 8%, and 14% configurations, respectively. The differences in electrical resistance measurements between specimen configurations at the same displacement excitation frequency are in part due to the influence of instantaneous stress applied at the beginning of harmonic displacement, which depend on the static strain characteristics of each configuration. This is discussed in Section 3.1 of the main text and Section 2 of the Supporting Information.

Additionally, as shown in Fig. 5(a) for the strain-sensitive specimen, resistance measurements increase between 3 and 50 Hz by +40%, +8%, and +4% for the ε = 4%, 8%, and 14% strain-sensitive specimen configurations, respectively. The trend of increasing resistance with frequency may be due to the frequency dependent properties of the FHE material systems. On the other hand, the amount of resistance change between displacement excitation frequencies for the same configuration depends on the static pre-strain characteristics. For instance, an increase in average output force according to displacement excitation frequency, as shown in Fig. 2(d), is due to the viscoelastic material properties of the specimens. Increases in average output force with displacement excitation frequency suggest that the state of stress and strain within the strain-sensitive specimen increase with frequency as well. To explore this further, FE model simulations are implemented to investigate how the strain rate that the ink trace experiences depends on the configuration and displacement excitation frequency, see Supporting Information Section 5. The frequency dependence of internal strain within the strain-sensitive specimen becomes manifest as increases in the state of strain within the conductive networks. Such growth of local strain acts to disrupt the conductive network and increases electrical resistance with increasing displacement excitation frequency. Furthermore, the influence of static strain characteristics can be seen in comparisons of the electrical resistance behavior between strain-sensitive specimen configurations. For example, the ε = 4% strain-sensitive configuration is in a state of greater maximum principal strain compared to the ε = 8% and ε = 14% configurations, see Fig. 2(a), which results in a greater change in resistance between displacement excitation frequencies.

It is important to note that the testing procedure may contribute to the frequency dependent resistance response of the strain-sensitive specimen in Fig. 5(a). After 2 min of applied harmonic displacement, a larger increase in resistance may be expected for a 50 Hz displacement excitation compared to a 3 Hz displacement excitation based on the number of displacement cycles that the conductive ink trace undergoes. Yet, if the number of displacement cycles determined the frequency dependent electrical resistance behavior in Fig. 5(a), the resistance measured for the ε = 14% configuration of the strain-sensitive specimen would be expected to decrease between 3 and 50 Hz, according to the results shown in Fig. 3(c). On the contrary, the resistance measurements of the ε = 14% strain-sensitive specimen increase by 4% between 3 and 50 Hz. This suggests that the frequency dependent resistance behavior of the strain-sensitive specimen in Fig. 5(a) is primarily due to the frequency dependent strain characteristics of the specimens, rather than the number of displacement cycles.

For the strain-insensitive specimen, the resistance measurements in Fig. 5(b) remain constant within 2% resistance change for all displacement excitation frequencies and specimen pre-strain configurations. The low static principal strains in the conductive ink trace beam associated with the strain-insensitive geometry, as shown in the FE model deformation shapes of Fig. 2(b), correspond to a similarly low dynamic strain influence on the conductive ink network. As a result, resistance measurements remain nearly constant, regardless of the frequency of the applied displacement and number of cycles. The results presented here further demonstrate how the static pre-strains contribute to the measured resistance change. With high static pre-strain, the strain-sensitive specimen configurations show frequency dependence through resistance changes of up to 40% between 3 and 50 Hz displacement excitation frequencies. With lower static pre-strains, the strain-insensitive specimen maintains resistance changes within 2% of the initial values for all configurations and displacement excitation frequencies considered.

4. Conclusions

Investigations into the dynamic properties of FHE material systems highlight the need to account for transient mechanical, electrical, and thermal influences manifest in material and geometry selections. Cyclic displacement experiments suggest that thermal heat generation within the conductive ink traces contributes to conductive network disruption and results in gradual resistance changes. In addition to the electric current flow, heat generation arises from thermal stresses in the ink that depend on differences in thermal expansion properties of the elastomer matrix and the silver microflakes suspended therein. The amount of heat generation is exacerbated by the pre-strain of the ink trace configuration. On the other hand, ink traces not subjected to high static pre-strains or high dynamic strain rates may exhibit an electrically robust conductivity that does not appear to degrade with increasing cycles of dynamic load. Finally, it is revealed that the magnitude of cumulative fatigue of the conductive ink traces is determined by the frequency of excitation due to the frequency dependent material properties and configuration dependent strain rates. As a result, one may envision exploiting a strain-sensitive FHE material system for resistance-based monitoring of dynamic response and cyclic stresses. Conversely, a nearly dynamic-independent conductivity may be cultivated by strain-insensitive FHE that delivers electrically robust properties even when subjected to high-cycle and high-frequency dynamic loads. These findings may guide attention to new concepts for FHE material systems exploited in applications involving periodic stress, such as wearables for motion monitoring and vibration isolation practices.

Acknowledgments

The authors acknowledge James Hardin of UES, Inc. and Jim Deneault of UTC for discussions and advice pertaining to specimen fabrication. This work is supported by the Air Force Research Laboratory and Dayton Area Graduate/Faculty Fellowship Program via grant number RX1-OSU-17-4.

Appendix A. Supplementary data

Supplementary data to this article can be found online at https://doi.org/10.1016/j.compstruct.2018.10.023.

References

[1] Bansal AK, Hou S, Kulyk O, Bowman EM, Samuel IDW. Wearable organic optoelectronic sensors for medicine. Adv Mater 2015;27:7638–44.
[2] Jiang H, Moon K, Li Y, Wong CP. Surface functionalized silver nanoparticles for ultrahigh conductive polymer composites. Chem Mater 2006;18:2969–73.
[3] Zhang R, Moon K, Lin W, Wong CP. Preparation of highly conductive polymer nanocomposites by low temperature sintering of silver nanoparticles. J Mater Chem 2010;20(10):2018–23.
[4] Valentine AD, Busbee TA, Boley JW, Raney JR, Chortos A, Kotikian A, et al. Hybrid 3D printing of soft electronics. Adv Mater 2017;29(40):1–8.
[5] Jeong S, Woo K, Lim S, Kim JS, Shin H, Xia Y, et al. Controlling the thickness of the surface oxide layer on Cu nanoparticles for the fabrication of conductive structures by ink-jet printing. Adv Funct Mater 2008;18:679–86.
[6] Chandra P, Singh J, Singh A, Srivastava A, Goyal RN, Shim YB. Gold nanoparticles and nanocomposites in clinical diagnostics using electrochemical methods. J Nanoparticles 2013;2013:1–12.
[7] Stauffer D, Aharony A. Introduction to percolation theory. 2nd ed. Philadelphia, USA: Taylor & Francis; 1994.
[8] Jahanshahi A, Salvo P, Vanfleteren J. Reliable strechable gold interconnects in biocompatible elastomers. J Polym Sci 2012;50:773–6.
[9] Wagner S, Lacour SP, Jones J, Hsu PI, Sturm JC, Li T, et al. Electronic skin: architecture and components. Physica E 2004;25:326–34.
[10] Borghetti M, Serpelloni M, Sardini E, Pandini S. Mechanical behavior of strain based on PEDOT:PSS and silver nanoparticles inks deposited on polymer subtrate by inkjet printing. Sens Actuators, A 2016;243:71–80.
[11] Das NC, Chaki TK, Khastgir D. Effect of axial stretching on electrical resistivity of short carbon fibre and carbon black filled conductive rubber composites. Polym Int 2002;51:156–63.
[12] Roberson DA, Wicker RB, MacDonald E. Microstructural characterization of electrically failed conductive traces printed from Ag nanoparticle inks. Mater Lett 2012;76:51–4.
[13] Shemelya C, et al. Anisotropy of thermal conductivity in 3D printed polymer matrix composites for space based cube satellites. Addit Manuf 2017;16:186–96.
[14] Lessing J, Morin SA, Keplinger C, Tayi AS, Whitesides GM. Stretchable conductive composites based on metal wools for use as electrical vias in soft devices. Adv Funct Mater 2015;25:1418–25.
[15] Khan S, Lorenzelli L. Recent advances of conductive nanocomposites in printed and flexible electronics. Smart Mater Struct 2017;26:1–23.
[16] Merilampi S, Bjorninen T, Haukka V, Ruuskanen P, Ukkonen L, Sydanheimo L. Analysis of electrically conductive silver ink on stretchable substrates under tensile load. Microelectron Reliab 2010;50:2001–11.
[17] Merilampi S, Bjorninen T, Ukkonen L, Ruuskanen P, Sydanheimo L. Embedded wireless strain sensors based on printed RFID tag. Sensor Review 2011;31:32–40.
[18] Wang X, Gu Y, Xiong Z, Cui Z, Zhang T. Silk-molded flexible, ultrasensitive, and highly stable electronic skin for monitoring human physiological signals. Adv Mater 2014;26:1336–42.
[19] Khan Y, et al. Flexible hybrid electronics: direct interfacing of soft and hard electronics for wearable health monitoring. Adv Funct Mater 2016;26:8764–75.
[20] Lau J, Schneider E, Baker T. Shock and vibration of solder bumped flip chip on organic coated copper boards. J Electron Packag 1995;118:101–4.
[21] Zhou Y, Al-Bassyiouni M, Dasgupta A. Vibration durability assessment of Sn3.0Ag0.5Cu and Sn37Pb solders under harmonic excitation. J Electron Packag 2009;131:011016.
[22] Wang P, Casadei F, Shan S, Weaver JC, Bertoldi K. Harnessing buckling to design tunable locally resonant acoustic metamaterials. Phys Rev Lett 2014;113:014301.
[23] Bishop J, Dai Q, Song Y, Harne RL. Resilience to impact by extreme energy absorption in lightweight material inclusions constrained near a critical point. Adv Eng Mater 2016;18:1871–6.
[24] Qi HJ, Boyce MC. Stress-strain behavior of thermoplastic polyurethane. Mech Mater 2004;37:817–39.
[25] Mulliken AD, Boyce MC. Mechanics of the rate-dependent elastic-plastic deformation of glassy polymers from low to high strain rates. Int J Solids Struct 2005;43:1331–56.
[26] Rittel D. On the conversion of plastic work to heat during high strain rate deformation of glassy polymers. Mech Mater 1999;31:131–9.
[27] Kultural SE, Eryurek IB. Fatigue behavior of calcium carbonate filled polypropylene under high frequency loading. Mater Des 2006;28:816–23.
[28] Harne RL, Wang KW. Harnessing bistable structural dynamics for vibration control, energy harvesting, and sensing. Chichester, UK: John Wiley & Sons Ltd; 2017.
[29] Mousanezhad D, Babaee S, Ebrahimi H, Ghosh R, Hamouda AS, Bertoldi K, et al. Hierarchical honeycomb auxetic metamaterials. Sci Rep 2015;5:1–8.
[30] Muth JT, Vogt DM, Truby RL, Menguc Y, Kolesky DB, Wood RJ, et al. Embedded 3D printing of strain sensors within highly stretchable elastomers. Adv Mater 2014;26:6307–12.
[31] Wang L, Ding T, Wang P. Effects of instantaneous compression pressure on electrical resistance of carbon black filled silicone rubber composite during compressive stress relaxation. Compos Sci Technol 2008;68:3448–50.
[32] Graz I, Cotton DPJ, Lacour SP. Extended cyclic uniaxial loading of stretchable gold thin films on elastomeric substrates. Appl Phys Lett 2009;94:071902.
[33] Herboth T, Guenther M, Fix A, Wilde J. Failure mechanisms of sintered silver interconnections for power electronic applications. Electronic Components and Technology Conference. 2013. p. 1621–7.
[34] Maiti SN, Ghosh K. Thermal characteristics of silver powder-filled polypropylene composites. J Appl Polym Sci 1994;52:1091–103.
[35] Busfield JJC, Thomas AG, Yamaguchi K. Electrical and mechanical behavior of filled rubber. III. dynamic loading and the rate of recovery. J Polym Sci 2005;43:1649–61.
[36] Yamaguchi K, Busfield JJC, Thomas AG. Electrical and mechanical behavior of filled elastomers. I. The effect of strain. Journal of Polymer. Physics 2003;41:2079–89.

Supporting Information

Title: Dynamic response of flexible hybrid electronic material systems

Nicholas C. Sears[(1)], John Daniel Berrigan[(2)], Philip R. Buskohl[(2)], and Ryan L. Harne[(1)]*

(1) Department of Mechanical and Aerospace Engineering, The Ohio State University, Columbus, OH 43210, USA

(2) Soft Materials Branch, Materials and Manufacturing Directorate, Air Force Research Laboratory, Wright Patterson Air Force Base, OH 45433, USA

** Corresponding author, email: harne.3@osu.edu*

1 Specimen fabrication

The specimen substrates are created in a 3D printer (Stratasys Objet260 Connex3) using a Stratasys PolyJet material, Tangoblackplus (FLX980). The conductive ink used for experimental specimens is composed of silver (Ag) microflakes (Inframat Advanced Materials, 47MR-10F) and a thermoplastic polyurethane (TPU) (BASF, 50126177). The Ag microflakes and TPU elastomer are combined and dissolved in an N-Methyl-2-pyrrolidone (NMP) solvent (Alfa Aesar, A12260). The conductive ink solution is sonicated for an hour at 60 rpm and centrifuged for 2 minutes at 2000 rpm before allowing the NMP to dissolve the TPU over the course of two days. The conductive ink solution is centrifuged for 2 minutes at 2000 rpm before every subsequent use. Once the combined mixture is applied to the specimens, the NMP evaporates and Ag-TPU ink remains. The Ag-TPU ink formulation used includes Ag microflakes that constitute 35% of the conductive ink volume (v%). Thus, the ink used in this research is 35v% Ag-TPU ink.

As shown in Figure S1(a), 34 gauge wire leads are connected to the ink trace on the surface of the experimental specimens via internal channels 1.4 mm in diameter. Channels for the wire leads are printed into the specimens and provide a stable connection for wire lead resistance measurements during dynamic excitation. Ag-TPU ink is applied to the experimental specimens with a syringe into a half-circle channel 0.4 mm in diameter printed into the face of the specimens. As exemplified in Fig. S1(a), additional Ag-TPU ink is injected into a small portion of the 1.4 mm internal channels to help ensure a strong connection at the location where the wire lead and ink meet. Epoxy (Hampton Research HR4-347) is injected into the end of the 1.4 mm internal channels where the wires leave the specimen in order to prevent movement between the wires and ink. Both the Ag-TPU ink and epoxy are allowed to cure at room temperature for 24 hours before experiments.

Overall dimensions for the strain-sensitive and strain-insensitive specimens are given in Figs. S1(b) and (c). As shown in Fig. S1(b), the Ag-TPU ink is applied on the vertical 2.2 mm beam of the strain-sensitive specimen. As shown in Fig. S2(c), the Ag-TPU ink is applied on the diagonal 1.8 mm member of the strain-insensitive specimen. Due to the soft nature of the Tangoblackplus material and the need to stabilize the prints during 3D printing, 1.8 mm plates made of Veroblackplus (RGD875) are printed on the top and bottom of each specimen. With the differences in Shore hardness values (Shore 26A and Shore 83D for Tangoblackplus and Veroblackplus, respectively), it is assumed that the thin Veroblackplus plates act as

rigid bodies with respect to the rest of the Tangoblackplus specimen. Therefore, strains for the strain-sensitive and strain-insensitive specimens are calculated with respect to heights of 22.9 mm and 22.1 mm, respectively. These dimensions correspond to the portion of the heights of each specimen composed of Tangoblackplus as seen in Fig. S1(b) and (c).

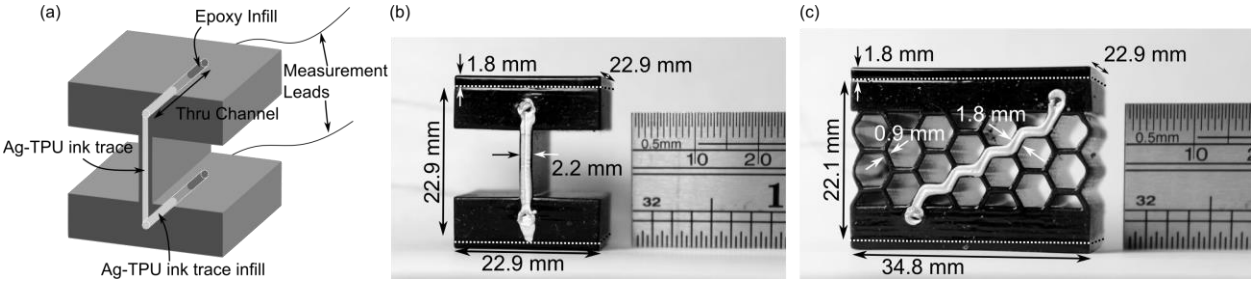

Figure S1. (a) Schematic of specimen fabrication constituents, shown specifically for the strain-sensitive specimen. Overall dimensions are shown for (b) the strain-sensitive specimen and (c) strain-insensitive specimen.

2 Viscoelastic hyperelastic material model parameter identification

To characterize the frequency and time dependent influences observed experimentally, a Prony series, viscoelastic hyperelastic material model is utilized. A cylindrical specimen of the same base material as the flexible hybrid electronic material system specimens undergoes DMA experiments in a mechanical spectrometer (TA Instruments ARES Rheometer). The DMA data in Fig. S2 is used to empirically identify the viscoelastic material model by the ABAQUS internal fitting routines for a Prony-series material model, with computed parameters shown in Table 1. The Prony series contributes to time dependent material behavior in accordance with (1) and (2). The g_i and the k_i are respectively the i^{th} shear and bulk relaxation coefficients, while τ_i is the i^{th} time relaxation constant. The constants $C_{10}^0 = \mu/2$ and $D_1^0 = 2/\kappa$ are respectively the instantaneous material properties of the hyperelastic material model.

$$C_{10}^R(t) = C_{10}^0\left(1-\sum_{j=1}^{N} g_j\left(1-e^{-t/\tau_j}\right)\right) \tag{1}$$

$$D_1^R(t) = D_1^0 / \left(1-\sum_{j=1}^{N} k_j\left(1-e^{-t/\tau_j}\right)\right) \tag{2}$$

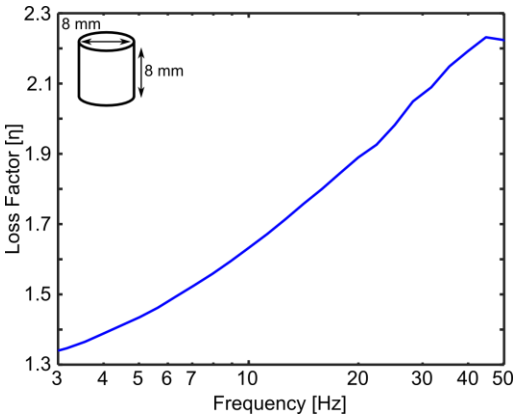

Figure S2. DMA experimental data from 3 to 50 Hz conducted on a Tangoblackplus cylindrical specimen used in ABAQUS FE models to generate the viscoelastic material model.

Table 1. Prony-series parameters computed by ABAQUS to generate the viscoelastic material model

i	g_i	k_i	τ_i
1	0.79215	0	0.00175
2	0.1202	0	0.0251
3	0	0.80177	0.00164
4	0	0.11483	0.0256

3 FE model studies for instantaneously applied stress in conductive ink traces

It is reported that instantaneously applied stress may result in a deterioration of conductive networks where larger stresses are associated with larger initial increases in resistance [1] [2]. This influence may contribute to the findings in Sec. 3.1 of the main text that show a 35% and 8% change in resistance by displacement cycle 100 for the ε=4% and 8% configurations of the strain-sensitive specimen, as shown in Fig. 3(c). Here, FE models of the specimens are used to characterize changes in von Mises stress experienced by the conductive ink traces at the beginning of a cyclic displacement experiment at 25 Hz. In order to model the experimental conditions, a downward displacement of 0.125 mm is applied to the specimens over the course of 0.02 seconds in a dynamic, explicit FE model formulation. The value of downward displacement 0.125 mm is the amount of downward displacement experienced by the specimens for half of a displacement cycle at 25 Hz, which takes 0.02 seconds to complete. Von Mises stress within the center of the beams onto which the conductive ink trace is applied, as shown in Fig. S1(b) and (c), is then monitored for the specimen geometries.

For the cyclic displacement experiments of Sec. 3.1 in the main text, the resistance change trends of Fig. 3(c) of the strain-sensitive specimen suggest that a rapid initial change in resistance occurs by displacement

cycle 100 for the ε=4% and 8% configurations. The FE model results in Figures S3(a) for the strain-sensitive specimen show that the ε=4% and 8% configurations are associated with changes in peak stress of 13100 Pa and 8500 Pa, respectively, after the application of the 0.125 mm displacement. On the other hand, the peak stress change of the ε=14% configuration is 3300 Pa. The resistances measured for the ε=14% strain-sensitive specimen in Fig. 3(c) do not indicate significant initial resistance increase and suggest that the resistance change of 1% by displacement cycle 100 may be more associated with applied cyclic displacements than with initial peak stress changes. The changes in peak stress for the ε=4% and 8% strain-sensitive specimen configurations in Fig. S3(a) represent approximately 400% and 260%, respectively, the change in peak stress experienced by the ε=14% configuration. The corresponding resistance changes of the ε=4% and 8% strain-sensitive specimen configurations at displacement cycle 100 are approximately 35% and 8% the values measured for the ε=14% configuration. Therefore, there may be underlying relations between instantaneous stress change and initial resistance change for the strain-sensitive FHE material system geometry.

For the strain-insensitive specimen, Fig. S3(b) shows peak stress changes of 1500 Pa, 1300 Pa, and 330 Pa for the ε=4%, 8%, and 14% configurations, respectively. The corresponding resistance change measurements in Fig. 3(d) do not indicate a large increase in resistance at the beginning of the experiments, and thus do not suggest that peak stress changes within the conductive ink traces of the strain-insensitive specimen contribute greatly to resistance changes.

The FE model findings of peak stress changes within the conductive ink traces suggest that they may contribute to the initial resistance changes shown in Figs. 3(c) and (d) of the main text such that larger changes in peak stress, Fig. S3, are associated with larger initial changes in resistance, the 100-cycle data in Fig. 3(c,d). Yet, future research should explore how specimen geometry and configuration contribute to resistance changes within conductive networks due to these initial transient sequences of dynamic load events.

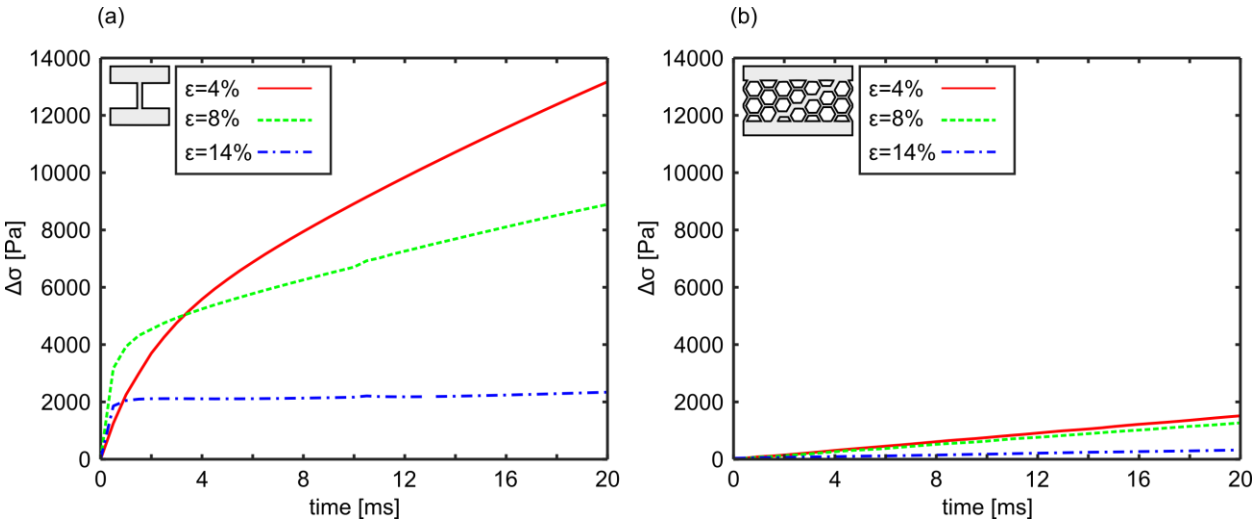

Figure S3. Change in ink trace stress for excitation applied at beginning of 25 Hz experiment for ε=4%, 8%, and 14% configurations of (a) strain-sensitive and (b) strain-insensitive specimens

4 Visual disruption of conductive ink network due to applied strain

For demonstrative purposes, 20% strain is applied to a Tangoblackplus substrate with a conductive ink trace on the center. The substrate is 41.5 mm x 17.5 mm x 2.6 mm in overall dimension, while the conductive ink trace is 27.2 mm x 2.5 mm in overall dimension and is aligned and centered on the substrate. Figures S4(a) and (b) show the conductive ink network before and after the applied strain, respectively, with inset schematics of the specimen included for reference. Disruptions to conductive ink trace networks, as shown in Fig. S4(b), change electrical resistance behavior and are noticeable as distortions to the original network in Fig. S4(a).

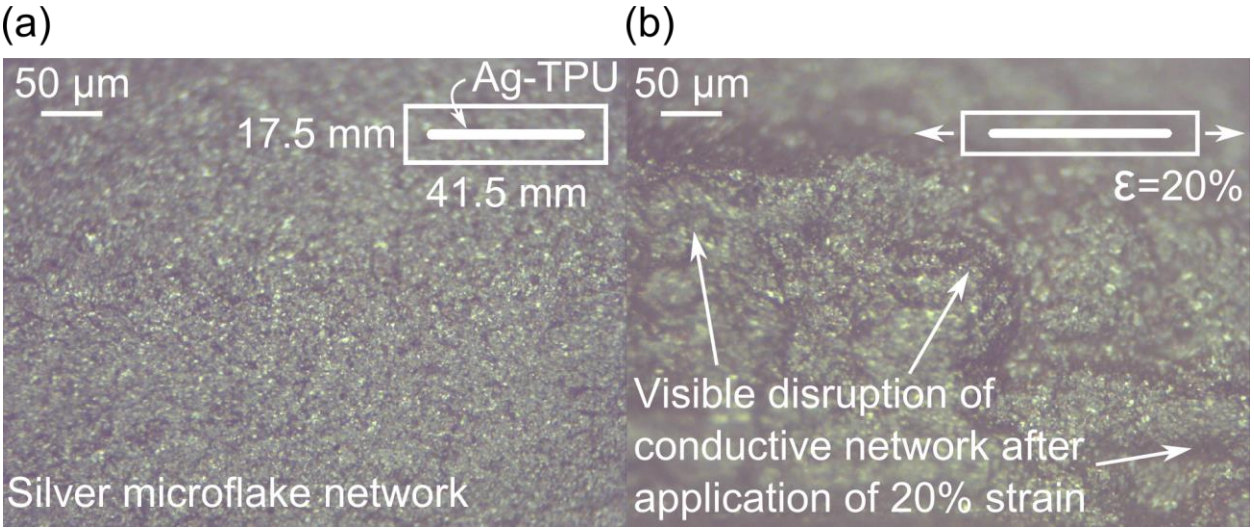

Figure S4. Visible disruption of a silver microflake network after 20% applied strain. Scale bars are 50 um.

5 Cyclic displacement experiments and modeling for specimens without conductive ink traces

As shown in Section 3.1 of the main text, the force transfer function of the specimens increases by less than 0.8% for all specimens and configurations by displacement cycle 10,000 in cyclic displacement experiments. In Section 3.2 of the main text, it is hypothesized that increases in force transfer function occur due to a softening of the elastomer material substrate of the specimen geometry. The softening of the substrate corresponds to a greater softening of input force compared to output force because the input side of the specimen is displaced whereas the outside side of the specimen is fixed.

In order to explore the influence that material softening may have on the force transfer function of the specimens and to eliminate the influence of the heat generated by the conductive ink trace, cyclic displacement experiments are performed on identical specimens without conductive ink traces. The experiments are conducted with 0.25 mm peak-peak applied displacement for 10,000 displacement cycles. The force transfer function is shown for the strain-sensitive and strain-insensitive specimens in Figures S5(a) and (b), respectively. Additionally, using the FE model described in Sec. 2.2 of the main text, the cyclic displacement experiments are modeled for the ε=4% configurations of the strain-sensitive and

strain-insensitive specimens for comparison. Note that the FE model described in Sec. 2.2 of the main text does not account for the thermoelasticity of the substrate material.

As shown in the experimental results of Figs. S5(a) and (b), the force transfer function increases for the strain-sensitive and strain-insensitive specimens by less than 0.8% for all configurations. The results in Figs. S5(a) and (b) resemble those in Figs. 3(a) and (b) of the main text for the specimens with conductive ink traces. Therefore, without the influence of the heat generated by the conductive ink trace, the results in Figs. S5(a) and (b) suggest that the changes in force transfer function measured in Figs. 3(a) and (b) are due to a softening of the elastomer material that makes up the specimen geometry, for which the displaced excited input side of the specimens softens more than the fixed output side. Furthermore, the FE model simulation results for the ε =4% configurations of both specimens in Figs. S5(a) and (b) shows a constant force transfer function with number of displacement cycles. The force transfer function computed in the FE model indicates that the changes in force transfer function measured experimentally for both specimens are due to internal heat generation of the elastomer material substrates, since the FE model does not account for these influences. The results shown in Fig. S5 conclusively identify the primary origins of the softening and heat generation of the specimen to be associated with the thermoelasticity of the substrate material instead of being associated with minor contributions from the Ag-TPU ink trace.

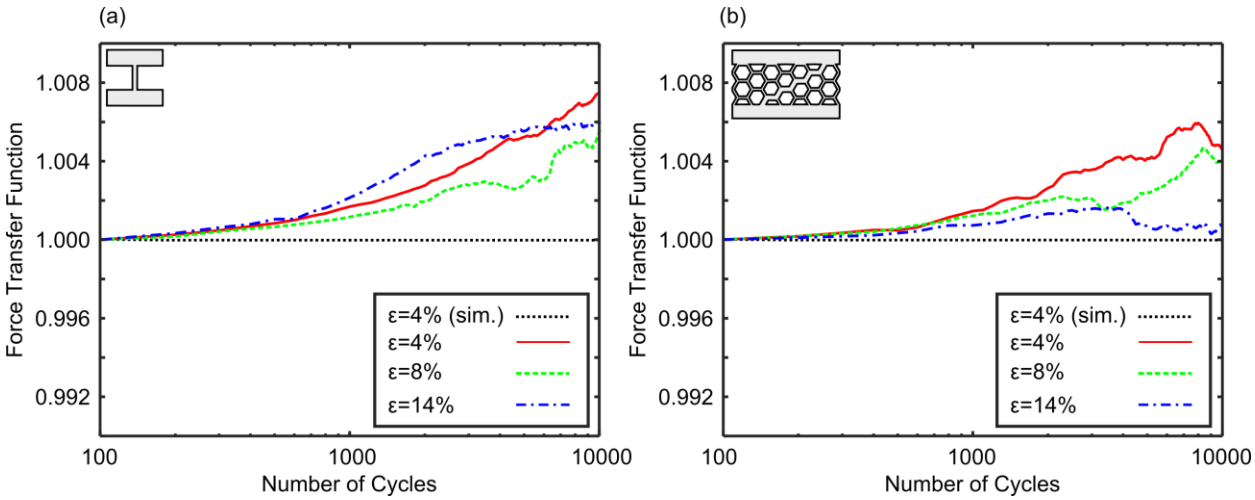

Figure S5. Force transfer function for cyclic displacement experiments conducted on specimens without conductive ink traces is shown for ε =4%, 8%, and 14% configurations of the (a) strain-sensitive and (b) strain-insensitive specimens for a 10,000 cycle displacement experiment with 0.25 mm peak-to-peak applied displacement. FE model simulation results for the cyclic displacement experiments are shown for the ε =4% configuration of both specimens as well.

6 FE model calculations for conductive ink trace strain rate

It is shown that cumulative damage in conductive networks increases with increasing strain [3] [4] and strain rate [5] [6] over the duration of cyclic displacement loading. These trends are thought to be due to stress propagation in the conductive networks. In order to investigate the potential of these influences on the conductive ink traces in this research, FE models of the specimens, as detailed in the Sec. 2.2 of the main text, are used to calculate the strain rate that the ink trace experiences under the various geometries

and configurations in this research. The strain rate of the conductive ink trace beam for each specimen and configuration is calculated for a 0.25 mm peak-to-peak harmonic displacement applied to the FE models of the specimens at displacement frequencies ranging from 3 to 50 Hz. In order to calculate the strain rate of the conductive ink traces, the peak-to-peak length changes of the conductive ink traces for each excitation frequency are calculated in the FE model and are normalized with respect to the length of the conductive ink trace under static conditions for each configuration. As shown in Figures S6(a) and (b) for the strain-sensitive and strain-insensitive specimens, respectively, FE model results show that the strain rate that the conductive ink trace experiences decreases with increasing specimen compression for both specimens. Additionally, strain rate is shown to increase with displacement frequency for all specimens and configurations. The FE model results presented here may have implications for the frequency dependence of resistance for the experimental specimens, such that increasing strain rates and displacement excitation frequency may result in increases in resistance.

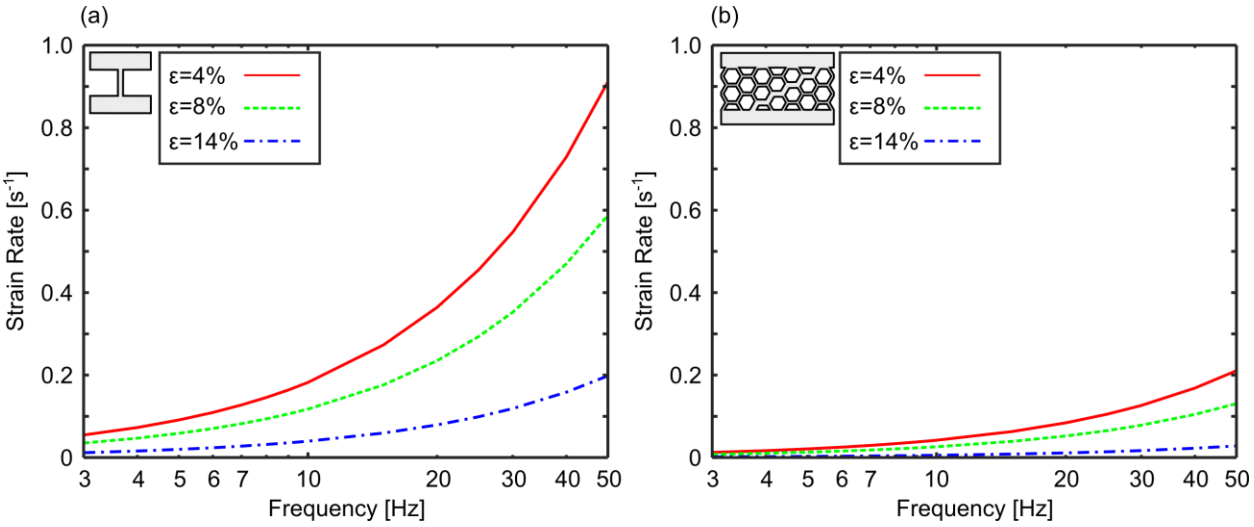

Figure S6. Strain rate of conductive ink trace according to excitation frequency and configuration for the (a) strain-sensitive and (b) strain-insensitive specimens

References

[1] J.T. Muth, D.M. Vogt, R.L. Truby, Y. Menguc, D.B. Kolesky, R.J. Wood, and J.A. Lewis, Embedded 3D printing of strain sensors within highly stretchable elastomers. Advanced Materials 26 (2014) 6307-6312.

[2] L. Wang, T. Ding, and P. Wang, Effects of instantaneous compression pressure on electrical resistance of carbon black filled silicone rubber composite during compressive stress relaxation. Composites Science and Technology 68 (2008) 3448-3450.

[3] A. Jahanshahi, P. Salvo, and J. Vanfleteren, Reliable strechable gold interconnects in biocompatible elastomers. Journal of Polymer Science 50 (2012) 773-776.

[4] S. Wagner, S.P. Lacour, J. Jones, P.I. Hsu, J.C. Sturm, T. Li, and Z. Suo, Electronic skin: architecture and components. Physica E: Low-dimensional Systems and Nanostructures 25 (2004) 326-334.

[5] M. Borghetti, M. Serpelloni, E. Sardini, and S. Pandini, Mechanical behavior of strain based on PEDOT:PSS and silver nanoparticles inks deposited on polymer subtrate by inkjet printing. Sensors and Actuators A: Physical 243 (2016) 71-80.

[6] N.C. Das, T.K. Chaki, and D. Khastgir, Effect of axial stretching on electrical resistivity of short carbon fibre and carbon black filled conductive rubber composites. Polymer International 51 (2002) 156-163.